Experimental Study on Structural Performance of Prefabricated Composite Box Girder with Corrugated Webs and Steel Tube Slab

He, Jun; Liu, Yuqing; Wang, Sihao; Xin, Haohui; Chen, Hongwei; Ma, Chaobo

DOI
10.1061/(ASCE)BE.1943-5592.0001405

Publication date
2019

Document Version
Final published version

Published in
Journal of Bridge Engineering

Citation (APA)
He, J., Liu, Y., Wang, S., Xin, H., Chen, H., & Ma, C. (2019). Experimental Study on Structural Performance of Prefabricated Composite Box Girder with Corrugated Webs and Steel Tube Slab. *Journal of Bridge Engineering*, *24*(6), Article 04019047. https://doi.org/10.1061/(ASCE)BE.1943-5592.0001405

Experimental Study on Structural Performance of Prefabricated Composite Box Girder with Corrugated Webs and Steel Tube Slab

Jun He, Ph.D.[1]; Yuqing Liu, Ph.D.[2]; Sihao Wang[3]; Haohui Xin, Ph.D.[4]; Hongwei Chen[5]; and Chaobo Ma[6]

Abstract: We present an innovative prefabricated composite box girder with corrugated webs and concrete-filled steel tube slab to prevent cracking in the web and reduce the self-weight, which is suitable for long-span structures. We carried out systematic experimental and analytical studies to investigate the structural performance, including the loading capacity and dynamic properties of a prefabricated composite box girder bridge before and after erection. Firstly, we tested a prefabricated composite girder with a single box section before erection under monotonic loading, measuring vertical deformation, flexural strain on the slabs, and shear strain on the corrugated steel webs, and evaluating the load-carrying capacity and stiffness reduction. Secondly, we conducted field live-load tests, including a calibration test and a dynamic test, on a composite bridge with twin prefabricated box girders. We hired four-axle heavy trucks for a calibration test to explore the static responses in terms of displacement, bending strain on the slabs, and shear strain on the corrugated steel webs. In the dynamic tests, we carried out a modal test using ambient vibration method and a moving load test in order to determine the dynamic behavior, which involves natural frequencies, the mode shapes, and the dynamic load factor (DLF). Based on the test results, the structural performance was evaluated by the AASHTO bridge rating process. All the findings from the load-carrying capacity test at ultimate state, calibration and dynamic load tests at service state in this study may provide a reference for the design and construction of such type of bridges. **DOI: 10.1061/(ASCE)BE.1943-5592.0001405.**

Author keywords: Composite bridge; Prefabricated girder; Corrugated steel web; Steel tube slab; Load-carrying capacity; Calibration load test; Dynamic load test.

Introduction

Bridges with short or medium span have been widely used in the past 100 years, often adopting reinforced or prestressed concrete solutions. It was proved that reinforced concrete bridges may have problems such as excessive cracking and heavy self-weight when applying for long spans (Nilson 1987). To this end, steel–concrete composite solutions with effective uses of both concrete and steel materials have been promoted and researched extensively (Brozzetti 2000; Nakamura et al. 2002). In addition, the application of prestressed strands in steel–concrete composite girders has been proved to be effective in controlling deflection and increasing the loading capacity, and therefore, there is increasing interest in this structure (Ayyub et al. 1992; Chen and Gu 2005). However, steel beams with high axial rigidity result in a low effectiveness in transferring prestressing, and they require excessive longitudinal or/and transverse stiffeners to prevent buckling instability. To solve these issues, Campenon Bernard BTP, France (Cheyrezy and Combault 1990) initiated the box or I-girder composite bridges using corrugated steel webs and prestressed tendons for bridge construction. A typical arrangement of a composite bridge with corrugated steel webs is given in Fig. 1, which includes top and bottom concrete slabs, corrugated steel webs, internal tendons, and external tendons with the deviators or the diaphragms. The principal advantages of the composite bridges adopting corrugated steel webs are summarized as follows: (1) reduced self-weight due to the replacement of concrete webs by corrugated steel webs may lead to reduced seismic forces and smaller substructures, thus resulting in reduction of construction cost; (2) the corrugated steel webs have higher shear buckling strength and out-of-plane flexural stiffness than that of the flat steel webs; (3) the corrugated steel web has a low axial rigidity, which can be stretched and contracted easily like an accordion (generally called the accordion effect of corrugated steel web), making prestressing efficiently being introduced into the top and bottom concrete slabs; (4) compared to conventional concrete web, a corrugated steel web can eliminate web stiffeners and construction formworks, and it is easier to assemble during construction, which improves construction efficiency and shortens construction time; (5) the external posttensioned tendons are easy to replace, offering convenience in bridge maintenance and retrofitting; and (6) the construction materials are used more efficiently because shear and bending forces are resisted optimally by the corrugated steel webs and concrete slabs, respectively (He et al. 2012a; Jiang et al. 2015).

[1]Associate Professor, School of Civil Engineering, Changsha Univ. of Science and Technology, Hunan, China (corresponding author). Email: frankhejun@gmail.com

[2]Professor, Dept. of Bridge Engineering, Tongji Univ., Shanghai, China. Email: yql@tongji.edu.cn

[3]Ph.D. Candidate., Dept. of Bridge Engineering, Tongji Univ., Shanghai, China. Email: wangsihao@tongji.edu.cn

[4]Research Fellow, Civil Engineering and Geosciences, Delft Univ. and Technology, Netherlands. Email: xinhaohui@126.com

[5]Engineer, Hunan Provincial Communications Planning, Survey and Design Institute Co. Ltd., Hunan, China. Email: skschenhongwei@163.com

[6]Senior Engineer, Xingtai Road and Bridge Construction Corporation, No. 79 Gao Zhuang Qiao Road, Hebei, China. Email: ma_chaobo@126.com

Note. This manuscript was submitted on February 28, 2018; approved on December 12, 2018; published online on April 9, 2019. Discussion period open until September 9, 2019; separate discussions must be submitted for individual papers. This paper is part of the ***Journal of Bridge Engineering***, © ASCE, ISSN 1084-0702.

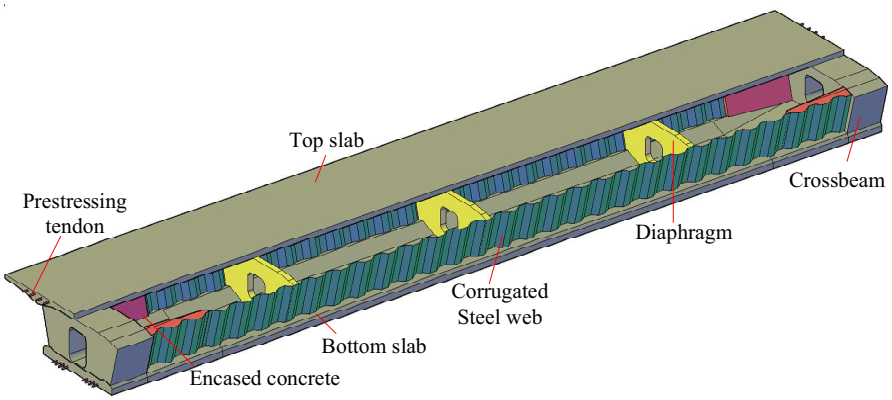

Fig. 1. Conventional composite bridge with corrugated steel webs.

Since the construction of the first highway bridge using corrugated steel webs (Cognac Bridge) in France in 1986, numerous composite bridges with corrugated steel webs have been erected worldwide. In addition, a considerable number of experimental and analytical studies have been carried out on such type of bridges, including studies on their bending behavior (Elgaaly et al. 1997; Mo et al. 2003; Huang et al. 2004; Kim et al. 2011; Elamary et al. 2017), shear behavior (Elgaaly et al. 1996; Luo and Edlund 1996; Driver et al. 2006; Yi et al. 2008; Sause and Braxtan 2011), torsional behavior (Mo et al. 2000; Mo and Fan 2006; Ding et al. 2012), fatigue behavior (Sause et al. 2006; Ibrahim et al. 2006), dynamic performance (Kadotani et al. 2003), and connection behavior (Kosa et al. 2006; Wang et al. 2018). In order to promote the application of such kind of bridges, He et al. (2012a) and Jiang et al. (2015) carried out a comprehensive review of relevant studies covering the significant research results about structural behavior, design, and construction methods.

To the authors' viewpoint, traditional plate or box girders with corrugated steel webs also have some drawbacks, such as: (1) potential shear buckling or large shear deformation of corrugated steel webs may occur around the supporting area in continuous girder bridges; and (2) significant local bucking of compressive flange or lateral–torsional buckling of corrugated steel web plate girder may appear under in-plane load. In order to improve the structural performance of corrugated steel webs in the supporting area, He et al. (2012b, c, 2014a, 2017) proposed partially encased composite girder with corrugated steel web and explored its shear and bending performance.

The application of tubular flanges or concrete-filled steel tubular flanges was proposed to improve the stability and load-carrying capacity of composite girders with corrugated steel webs (Wang 2003; Sause et al. 2008) because substituting the flat single-plated flange with the tubular flange can improve the twisting strength of the beams with open sections and decrease their sensitivity to lateral–torsional buckling. The first engineering instance of this structure is the Maupré Bridge, which consists of a box girder of triangular section, a concrete-filled tubular bottom flange, and a prestressed concrete deck (Johnson et al. 1997). The excellent structural properties of the I-girder with tubular flanges and corrugated webs have been verified by experimental and numerical investigations (Shao and Wang 2016, 2017; El Hadidy et al. 2018). However, previous studies focus on the plate girder with tubular flanges and corrugated webs, and prestressed strands were not arranged into the concrete-filled steel tube. In order to control the deflection and stress at the serviceability limit state and improve bending and torsional capacity, a prefabricated composite box girder with corrugated webs and

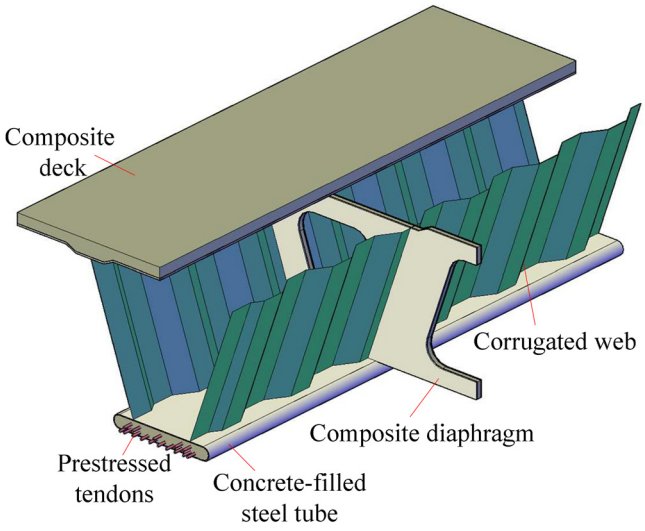

Fig. 2. Prefabricated composite box girder with corrugated webs and steel tube slab.

prestressed concrete-filled steel tube slab was introduced (Chen 2013; He et al. 2014b). As presented in Fig. 2, this new type of composite system consists of the superimposed concrete slab with steel plate, corrugated steel webs, a steel diaphragm, and a rounded-ended rectangular tubular bottom flange filled with prestressed concrete. Prestressing can be efficiently applied to the concrete slabs due to corrugated webs' accordion effect. In addition, the steel tube is filled with concrete for the aims of transferring prestressing and avoiding the buckling of thin-walled steel tube. Prestressed strands are protected by an additional external layer of the steel tube to improve strand durability and prevent their possible deterioration due to concrete crack. In order to have a high quality of concrete pouring in the steel tube, self-compacting concrete with a high mobility and the nonsegregated property was used. Mechanical vibration is not needed in the construction for this kind of concrete. Also, some air-bleed holes were opened and checked during the concrete pouring process to avoid voids occurrence. Steel–concrete composite slab, which consists of a thin steel plate at the bottom and reinforced concrete on the top, was adopted as the deck system. This steel plate in the composite slab can serve as formwork for concrete casting and is combined with concrete by the bent-up reinforcements. The corrugated steel webs were connected to the top and bottom flanges by welding; thus, no additional connectors were needed. The fatigue behavior of welding joints between corrugated steel webs

and flange plates have been experimentally and numerically studied (Anami and Sause 2005; Anami et al. 2005; Wang and Wang 2014). The results revealed that fatigue cracks initiated at the weld toe of the external weld line and propagated through the main plate thickness, in addition, increasing the bend radius (i.e., transition curvature), and flange thickness could lead to a decrease in the weld toe stress and an increase in fatigue life. Therefore, using reasonable corrugation profile and tubular flange can improve the fatigue performance of the welding connections. Steel diaphragms were arranged at specific spaces to connect two or more prefabricated composite box girders transversally and increase the lateral stiffness of the whole structure.

The fabrication process of the prefabricated box girder bridge is given in Fig. 3. Before erection, all the steel structural components

Fig. 3. Fabrication of prefabricated composite box girder bridge: (a) welding of the steel tube; (b) product of steel diaphragm; (c) installation of corrugated steel webs; (d) installation of steel plate; (e) composite deck before concrete casting; (f) prestressing; (g) connecting fabricated girders by diaphragms; and (h) finished state.

are fabricated and assembled in the factory. The prefabricated box girders are then transported to the construction field and connected by welding the steel diaphragms. Finally, without any formworks or supporting posts for the deck system, concrete is directly cast on the steel plate and connected to the steel plate through the bent-up bars and reinforcing bars, saving construction time and cost (He et al. 2014b). Therefore, these prefabricated box girders are very suitable for accelerating bridge construction.

In order to explore the static and dynamic behavior of this newly proposed composite structure, we performed both experimental (including model test and field test) and theoretical analyses. We tested a prefabricated composite girder with single box section before erection under monotonic loading (He et al. 2014b), and the test results confirmed that the prefabricated composite girder had enough load-carrying capacity and ductility. However, the structural performance of a composite bridge with multiple prefabricated box girders after erection is different from that of a composite bridge with a single box girder before erection. Hence, we conducted field live-load tests, including a calibration test and a dynamic test on a composite bridge with twin box girders, to explore the static behavior in terms of the deformation and strain distributions, as well as the dynamic behavior in terms of natural frequencies, mode shapes, and dynamic load factor (DLF) at serviceability state. Finally, we evaluated the structural performance using a code-based rating process through the test results.

Load-Carrying Capacity Test at Ultimate State

We tested a prefabricated composite box girder with corrugated steel webs and concrete-filled steel tube slab (30 m long, 1.8 m high, and 3.5 m wide) before erection under monotonic loading (Fig. 4), and we checked its load-carrying capacity and ductility by a full-scale loading test.

For the test specimen, the concrete used in bridge deck and tube slab had a specified 28-day compressive strength of 39.1 MPa and Young's modulus of 3.28×10^4 MPa. The steel components included steel flanges, corrugated steel webs, steel tube, and adopted weathering steel [Q355qENH (ANSTEEL, Liaoning Province)] with the tensile yielding strength of 410 MPa and ultimate strength of 540 MPa. The reinforcements used steel [HRB335 (ANSTEEL, Liaoning Province)] with the nominal tensile yielding strength of 335 MPa. The Young's modulus of steel components and reinforcements was 2×10^5 MPa. The posttensioned strands using low-relaxation steel had a specified yield and ultimate strength of 1,650 and 1,860 MPa, respectively, and Young's modulus of 1.95×10^5 MPa. The details of geometrical parameters, loading process, and measurement instruments can be referred to the authors' previous study (He et al. 2014b); only some important test results are reproduced here.

The relations between applied load and midspan deflections are given in Fig. 5. The deflection increases linearly with the applied load up to 1,420 kN when the concrete in the bottom steel tube is cracking. Afterward, the flexural rigidity deteriorates, leading to an obvious increase of the deflection. During the whole loading process, we measured relative slip between concrete slab and steel plate of the deck at support section to be less than 0.1 mm, indicating that concrete slab can be fully connected to the steel plate with the help of bent-up bars as shear connectors. Table 1 summarizes test results of maximum deflection, normal stress of top concrete slab and bottom steel tube at midspan section, and shear stress of corrugated steel web near the support section under different loading stages. In the table, the design load was determined according to the specification JTG D62 (Ministry of Communication of China 2012), while the serviceability state was defined as the maximum deflection

(a)

(b)

Fig. 4. Load-carrying capacity test of a prefabricated composite box girder before erection: (a) test specimen; and (b) test setup and loading.

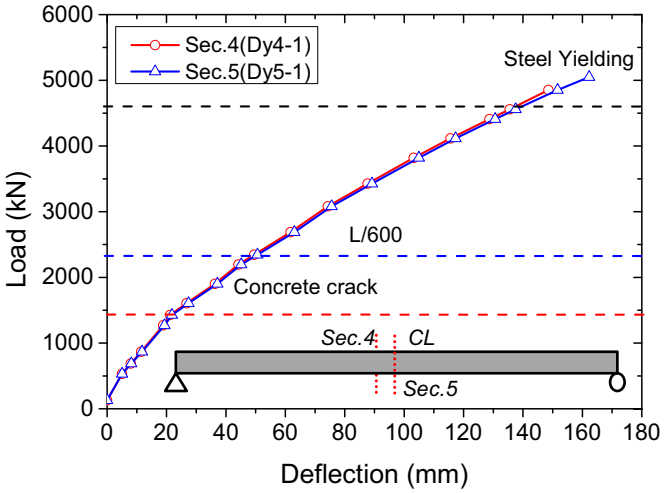

Fig. 5. Load–displacement relationship.

reached to $L/600$ (L is the total span of the girder). The design load was much less than the applied load at concrete cracking, which means that the composite girder was at the elastic state. In addition, the normal stress of bottom steel tube at midspan (Section 5) and shear stress of corrugated steel web near support (Section 2) are much less than the allowable values (355 MPa for tension and 205 MPa for shear) at serviceability state. The applied load till the yielding of the steel tube is about 5.5 and 2 times the load at the

Table 1. Test results at different loading stages

Stage	Load (kN)	Bending moment (kN·m)	Deflection (mm)	Concrete compressive stress (MPa)	Steel tensile stress (MPa)	Shear stress of web (MPa)
Design load	875	3,281	11.8	4.0	30	15
Concrete cracking	1,420	5,218	21.8	7.1	56	27
Serviceability state	2,344	8,614	50.0	9.8	155	47
Steel yielding	4,853	17,834	151.7	18.2	412	85
Ultimate state	5,050	18,560	167.2	20.1	419	92

design and serviceability states, respectively, while the corresponding maximum deflection at midspan section is about 13 and 3 times, respectively. Thus, the prefabricated composite box girder has enough load-carrying capacity and sufficient ductility.

The normal strain of the slabs at midspan (Section 4) and the shear strain of the corrugated steel web near the end support along the height of the girder are given in Figs. 6 and 7, respectively. The normal strain on the corrugated web was very small, even after the yielding of the bottom steel tube, which verified the accordion effect of corrugated steel web. Therefore, flexural strength was almost resisted by the top and bottom slabs, with negligible contribution from the corrugated steel webs. The shear strain distributed almost uniformly along the height of the web. Some data at the bottom of the web were lost because Gauge Sw2-3 failed unexpectedly after loading of 2,500 kN. The maximum shear strain of the web was much less than the yielding strain, indicating that the corrugated steel webs were still in the elastic stage, and no shear buckling appeared until the ultimate state.

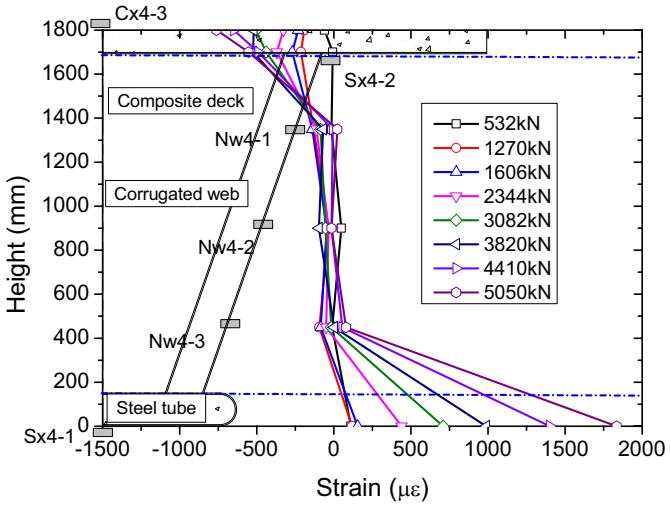

Fig. 6. Normal strain distribution along the height of Section 4.

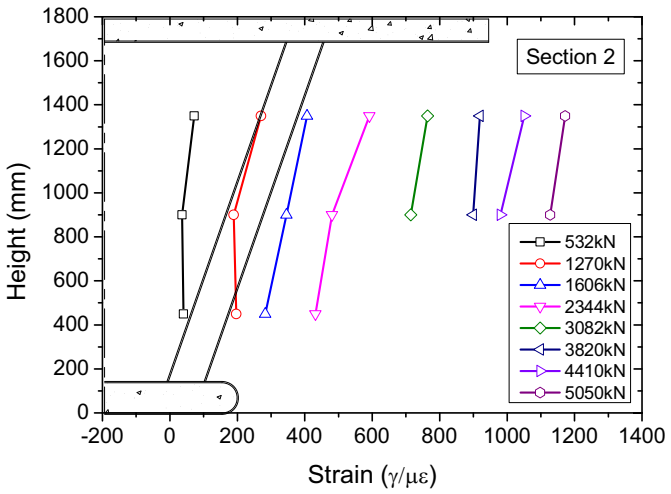

Fig. 7. Shear strain distribution along the height of corrugated web.

Live-Load Filed Test at Serviceability State

Description of the Prefabricated Bridge after Erection

The test bridge was a composite bridge consisted of two prefabricated box girders, having a length of 30 m and a width of 7.4 m. The test bridge was simply supported, as presented in Fig. 8. The superstructure included double box girders, which were connected by the steel diaphragms. Before erection, each box girder had the same dimension as the test specimen in load-carrying capacity test did. Two end diaphragms with a thickness of 160 mm and seven intermediate diaphragms with a thickness of 120 mm were arranged to improve the load distribution in the transverse direction. These diaphragms encompassed the entire depth of the box girder and were tied into the top and bottom flanges. The material properties of the concrete and steel of the tested bridge were the same as that of the test specimen in load-carrying capacity test.

Live-Load Test Procedure

Bridge field testing has become an acceptable means to determine a more accurate estimate of a bridge's safety capacity (Lichtenstein 1993). This technique can partially overcome the uncertainties associated with actual material properties, bridge field condition, and assumptions used during the bridge's' design, resulting in a powerful tool that provides a better understanding of the bridge behavior in its actual field condition. The results obtained from the field test can be used to study various structural characteristics of the bridges (Cai and Shahawy 2003; Eom and Nowak 2001; Ashebo et al. 2007; Teixeira de Freitas et al. 2012, 2017).

In this study, we carried out three kinds of field tests: calibration, modal, and DLF tests. We carried out the calibration test to relate the reading of strain and displacements recorded from the gauges (to obtain the calibration factor) under the known actual load of the calibration trucks. We mainly conducted the modal test to determine the dynamic behavior, including the natural frequencies, mode shapes, and damping ratios. We performed the DLF test to explore the bridge–vehicle interaction and determine the appropriate value of DLF for the design purposes.

Calibration Truck

We hired a truck with known gross weight, axle weight, axle spacing, and wheel spacing for the calibration test. We chose two kinds of the truck in the field test; one was four axles (gross weight ~48 ton) for

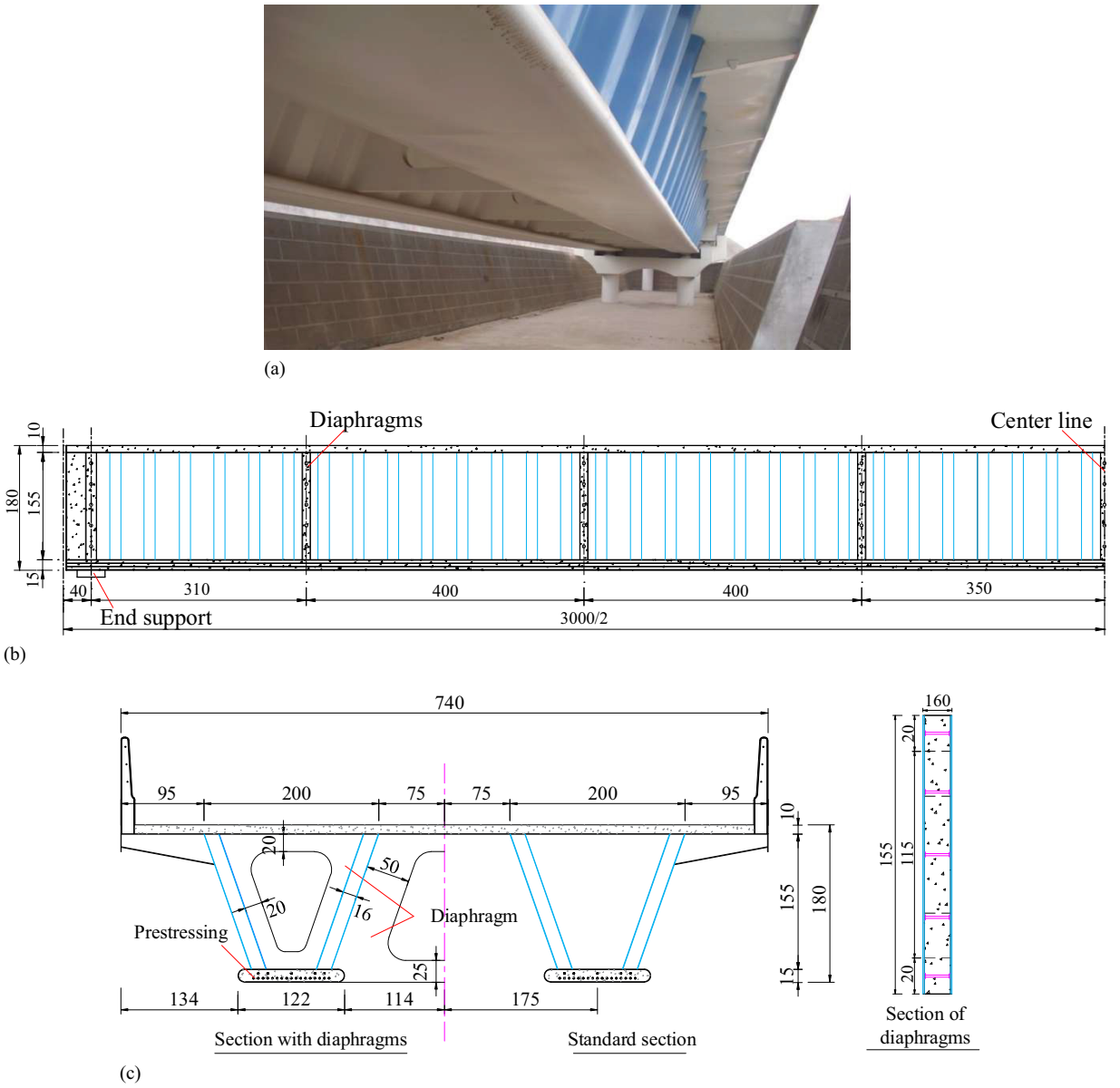

Fig. 8. Composite box girder bridge with corrugated steel webs (unit: cm): (a) tested bridge; (b) elevation view; and (c) cross section.

static loading, and the other was three axles (gross weight ~30 ton) for dynamic loading, as given in Fig. 9. For static loading, we placed two 48-ton trucks at the predetermined position, while for dynamic loading, we moved a 30-ton truck through the bridge with speeds of 20, 30, and 40 km/h, respectively. We measured the total gross weight of the vehicle and the weight of each axle in a weighing station before these tests. The spacing between the axles is given in Fig. 9, and the width of the axles of the truck was 1.86 m.

Loading Procedure

In the calibration test, we located the rear axle of the truck at the measured section according to the influence line of internal forces. Five load cases were considered in static loading test: two load cases were measuring the maximum shear force ($V_{max.}$) at the supported section; both symmetrical (Sym.) and eccentric (Ec.) loading were considered. Two other cases were estimating the maximum bending moment ($M_{max.}$) at the middle section; also, symmetrical and eccentric loading were involved. For the rest of static load case, we applied an eccentric loading to check the local deformation of the cantilever deck.

Ambient vibration testing using the traffic and wind as natural excitation is less costly than forced vibration testing, since no extra equipment is needed to excite the structure. However, relatively long duration records of the response measurements are required; the magnitudes of the parameters measured are rather small; consequently, high-frequency modes typically are not captured (Ren et al. 2004). The tested bridge was a simply supported girder bridge; only the low-frequency modes were concerned. Therefore, we conducted ambient vibration testing to determine dynamic parameter characteristics, including the natural frequencies, mode shapes, and damping ratios.

We carried out the DLF tests under a moving load to collect data on the vehicles-induced responses of the bridge. A three-axle truck (gross weight ~30 ton) was moving at the speeds of 20, 30, and 40 km/h to obtain the dynamic response in terms of strain and deflections at the middle span. A 30-ton truck jumped down from a wedge-shaped block with a height of 10 cm to simulate the local damage of the deck and dynamic strain, and we measured

deflections to investigate the impact factor. All the load cases and tested contents are summarized in Table 2. The arrangement of the calibration trucks in these tests is given in Fig. 10.

Instrumentation and Data Acquisition

We collected the static and dynamic responses of the bridge using different kinds of sensors, namely strain gauges, accelerometers, and displacement transducers (e.g., linear variable differential transformers; LVDTs), as given in Fig. 11. We measured the normal strain on the top of the concrete deck and the bottom of the steel slab at midspan section (Section 4), including dynamic strain gauges [G'4–1 ∼ 3 (Kingmach Measurement & Monitoring Technology, Hunan Province)]. We glued strain rosettes on the corrugated steel web at the end section (Section 1) to observe the shear strain. We measured static and dynamic deflections on the bottom of steel slabs by D4-1 and D'4-2 ∼ 3 at midsection (Section 4), respectively. In addition, to investigate the local deformation of the bridge deck, we installed displacement gauges at the bottom of the deck in Section 2, as given in Fig. 11(c).

We instrumented seven locations with biaxial accelerometers (one accelerometer was in the transverse direction, while the other was in the vertical direction; there were 14 accelerometers in total) for collecting dynamic data to determine the natural frequencies, mode shapes, and damping constants, as given in Fig. 11(d). We recorded the ambient acceleration–time histories for 120 s at intervals of 0.01 s, and we recorded the measurements of all accelerometers at the same time. We repeated the ambient vibration measurements three times in order to ensure the repeatability of the identified results.

All the information obtained from the LVDTs, strain gauges, and accelerometers were automatically recorded by a data acquisition system at regular intervals.

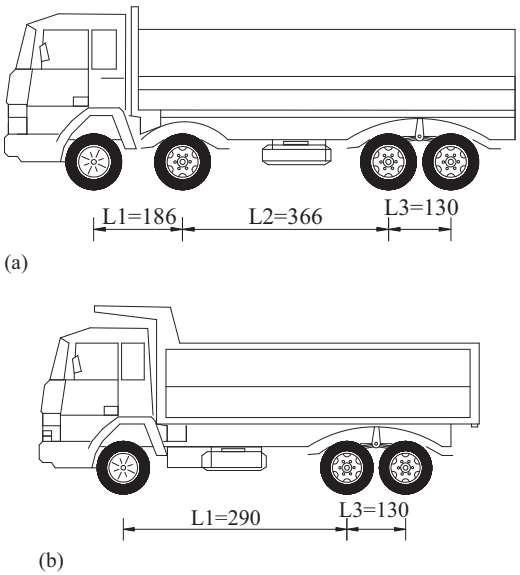

Fig. 9. Calibration truck (unit: cm): (a) 48 ton; and (b) 30 ton.

Finite-Element Models

The finite-element analysis (FEA) program ANSYS (version 13.0) was used to model the static and dynamic loading tests. We used solid elements, shell elements, and link elements to simulate the concrete deck, steel girder, and prestressed tendons, respectively; the FE model is given in Fig. 12. For the concrete slab, we used the eight-node 3-D reinforced concrete solid elements (SOLID65). We assumed the reinforcing bars in concrete slab to be smeared throughout the solid elements with volume ratios. Since the bridge in live-load field test was at the elastic state, the stress–strain relationship of the concrete was taken as linear.

The steel components, including corrugated steel webs, steel tube, and steel diaphragms, were simulated by the eight-node structural shell elements (SHELL93). The stress–strain relationship of steel components was taken as elastic-perfectly-plastic and incorporated into the FE model with the bilinear kinematic hardening (BKIN) option.

The prestressed tendons were modeled by the two-node 3-D spar elements (LINK8). The perfect bond between prestressed tendons and surrounded concrete was assumed. The relative slip was ignored through sharing the nodes of the SOLID65 elements with those of the LINK8 elements. An initial strain was given in the LINK8 element to simulate prestressing force.

All the material properties in FE simulation adopted the corresponding value in material tests. The tested bridge was simply supported on the bearings and subjected to concentrated loads over the contact area through the wheel print, which we simulated the same way as field load tests. We followed a step-by-step linear analysis to analyze the bridge model under the loads imposed by the trucks during the field load tests.

Calibration Test Results

We carried out the static calibration tests to determine the calibration factors according to the comparison between the measured responses (displacement or strain) and the calculated ones. Before each calibration test record, we made the data acquisition system run autozero; then we asked the calibration trucks to approach up the bridge deck, stop, and align at the specified location to record the static responses of the strain and displacement.

After recording bridge responses under applied loads of calibration trucks at each location, we compared the simulated results from

Table 2. Load cases and test contents

Load Case	Test type	Test content	Truck arrangement	Number of trucks	Measurement items
1	Static test	V_{max} at support	Sym. load	2	Shear strain
2		M_{max} at middle span	Sym. load	2	Normal strain, displacement
3		V_{max} at support	Ec. load	2	Shear strain
4		M_{max} at middle span	Ec. load	2	Normal strain, displacement
5		Transverse M_{max}	Ec. load	1	Displacement
6	Dynamic test	Modal test	Sym. load	1	Acceleration, frequency, modal shape
7		Moving load test	Sym. load	1	Normal strain, displacement
8		Impact load test	Sym. load	1	Normal strain, displacement
9		Braking load test	Sym. load	1	Normal strain, displacement

Note: Ec. = eccentric; and Sym. = symmetrical.

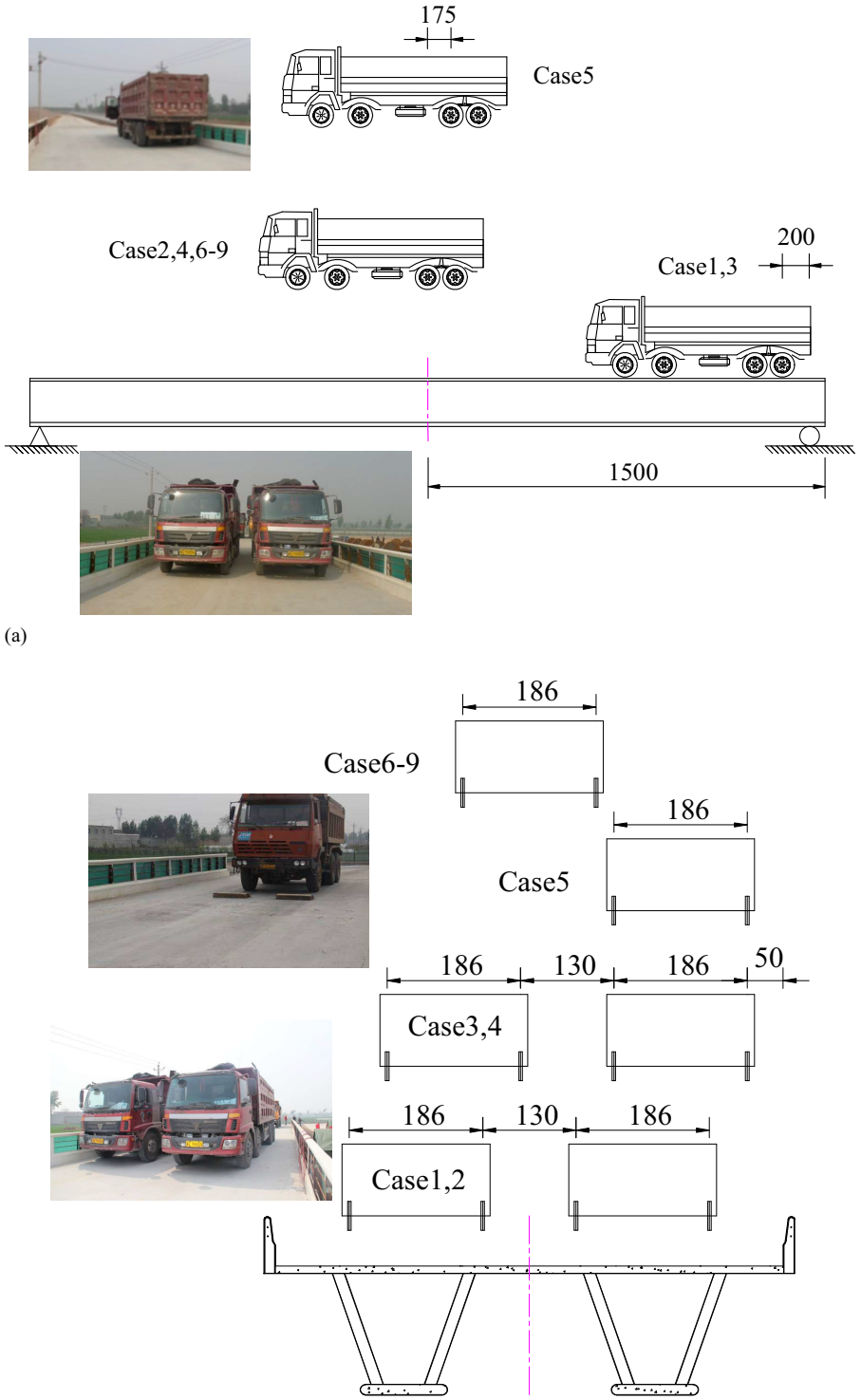

Fig. 10. Load cases for field tests (unit: cm): (a) side view; and (b) section view.

FEA to the tested ones. We obtained the calibration coefficients (η) by computing the ratio of the measured responses (S_t) to the simulated (FEA) ones (S_f). The calibration coefficient is an important indicator to assess the structural safety.

Displacements

The vertical displacements at the middle span (Sections 3 and 4) under Load Cases 2 and 4 are given in Fig. 13. In addition, the vertical displacements at Section 2 under Load Case 5 are given in Fig. 14 to check the local deformation of the cantilever deck. The displacements from the experimental results followed the same pattern as those obtained from the FE analytical results; both measured and calculated deflections distributed uniformly under Load Case 2 (symmetrical loading), but the deflections distributed unevenly along the transverse direction under eccentric loading (Load Cases 4 and 5), and the deflections reduced almost linearly as the increase

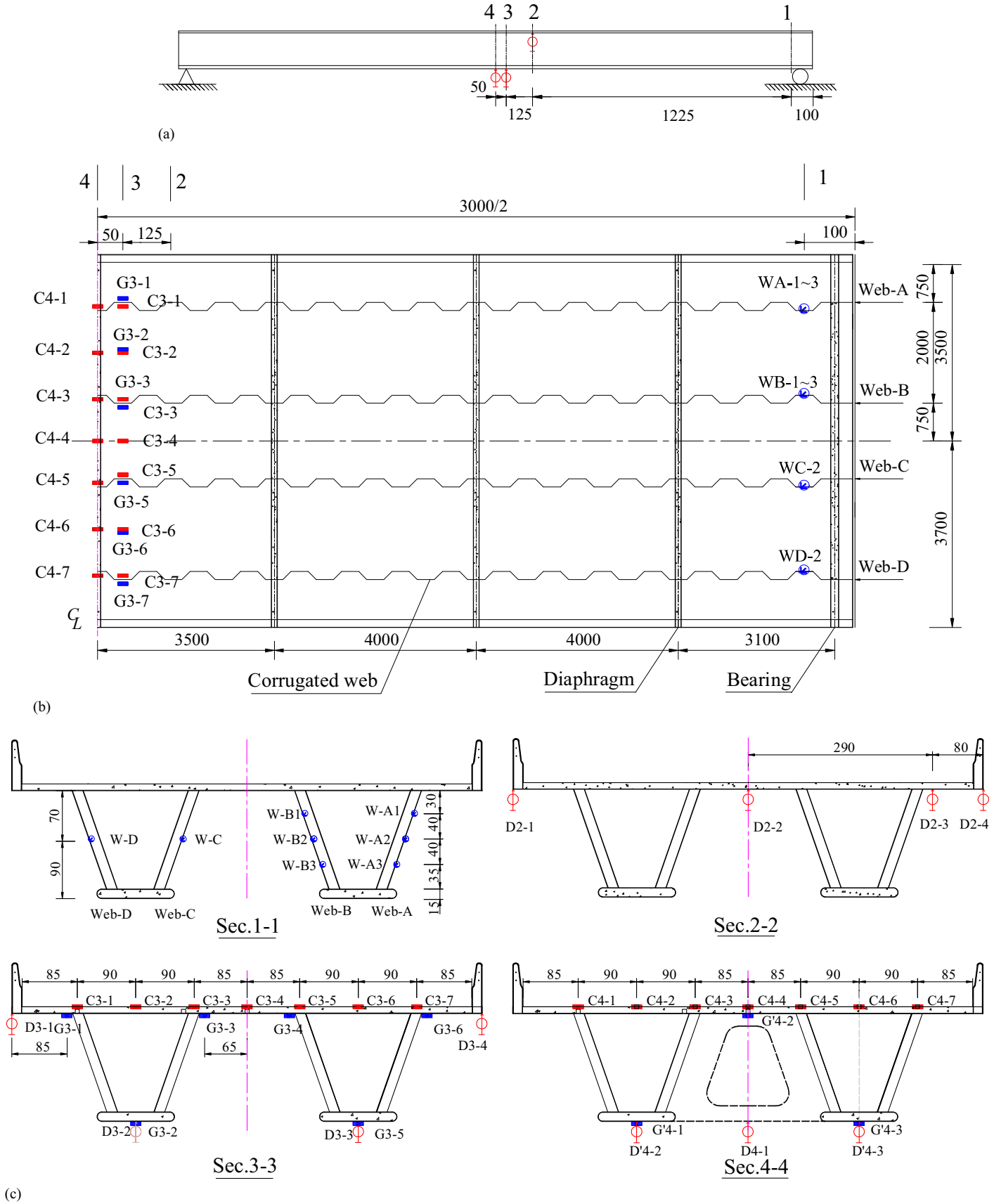

Fig. 11. Layout of instrumentations for field load tests (unit: cm): (a) displacement gauges arrangement: side view; (b) strain gauges arrangement: top view; (c) displacement and strain gauges arrangement: section view; and (d) accelerometer arrangement.

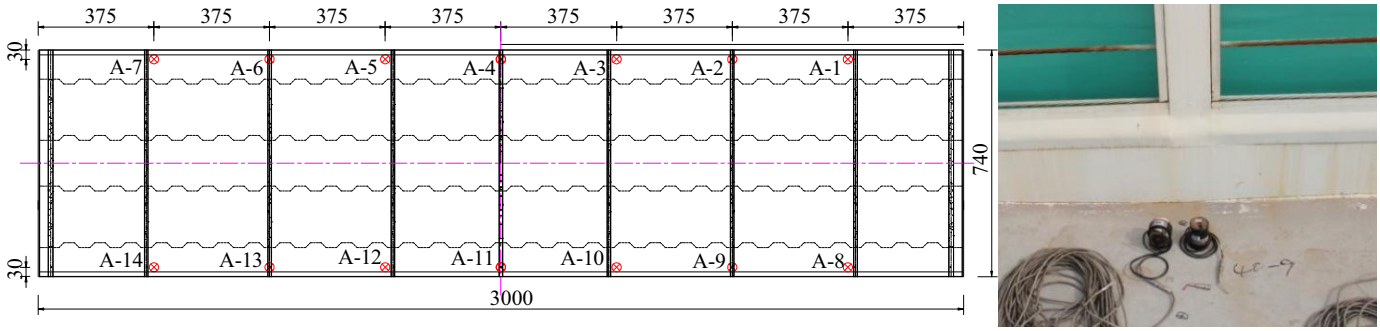

(d)

Note: - Displacement transducers - Strain gauge on concrete - Accelerometer

- Strain rosette - Strain gauge on steel

Fig. 11. (*Continued.*)

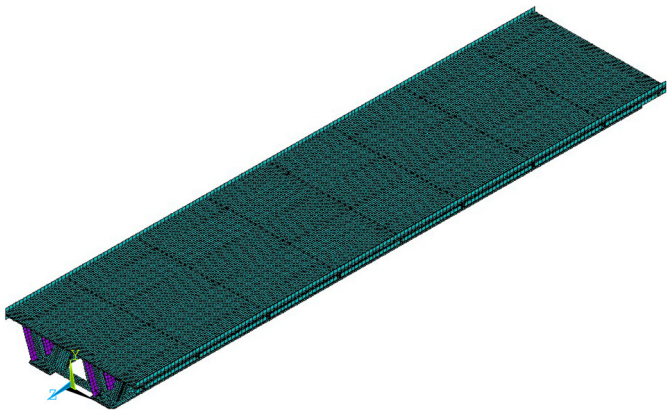

(a)

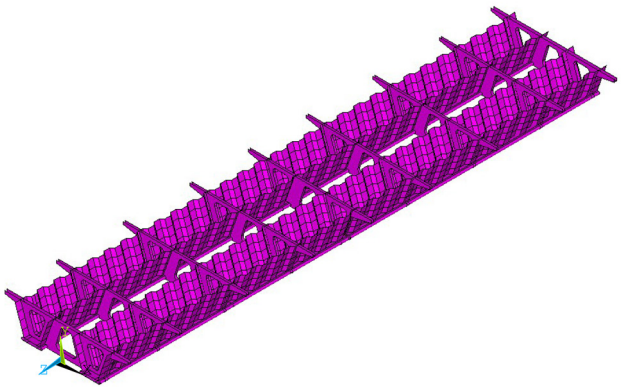

(b)

Fig. 12. Finite-element model: (a) whole bridge; and (b) steel components.

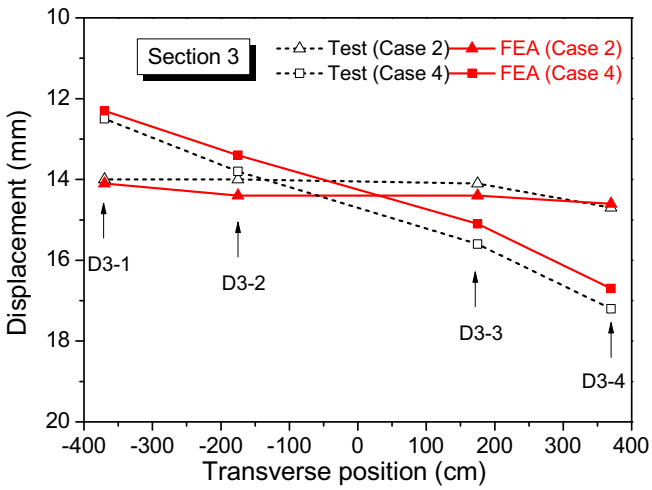

Fig. 13. Displacement distribution in Section 3 (Load Cases 2 and 4).

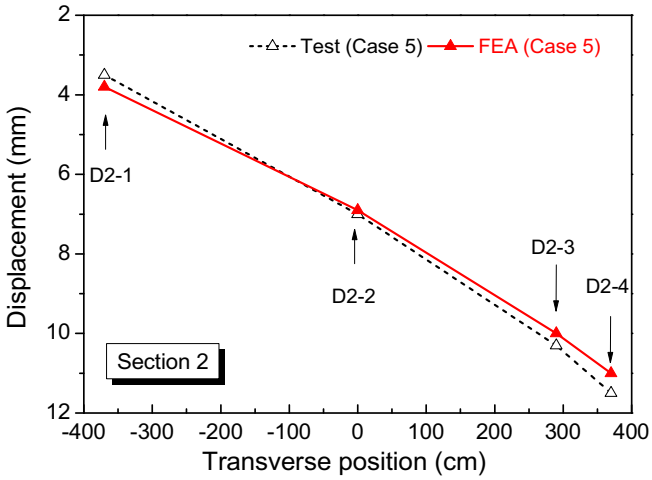

Fig. 14. Displacement distribution in Section 2 (Load Case 5).

of the distance from applied load. In order to consider the effect of unbalanced load, the eccentric coefficient of deflection (δ_e) was defined as the ratio of maximum deflection under eccentric loading to that under symmetrical loading, δ_e = 17.2 mm (Load Case 4)/ 14.7 mm (Load Case 2) = 1.17. Additionally, the η of displacements changed from 0.92 to 1.05 (the minimum and maximum η

were obtained from the deflection of D2-1 under Load Case 5 and D2-4 under Load Case 5, respectively), indicating that the calculated deflections from FEA agreed well with the measured ones under both symmetrical and eccentric load conditions, and the maximum deflection (17.2 mm) was much less than the limit value under the serviceability state ($L/600 = 50$ mm) (JTG D62; Ministry of Communication of China 2012), which confirmed that the tested bridge had enough stiffness.

Normal Strain on Slabs

The normal strain on the concrete slab at the middle span (Sections 3 and 4) under Load Cases 2 and 4 are given in Fig. 15. Both measured and calculated normal strain distributed uniformly along the transverse direction of the cross section under Load Case 2 (symmetrical loading); while the normal strain distributed unevenly under eccentric loading (Load Case 4). Moreover, the effect of the unbalanced load at Section 3 without steel diaphragm was more obvious than that at Section 4 with steel diaphragm, since the steel diaphragms improve the lateral stiffness and help the distribution of the eccentric load in the transverse direction by connecting two box girders together.

The η of concrete normal strain changed from 0.92 to 1.07 (the minimum and maximum η were obtained from the concrete strain of C3-3 under Load Case 4 and C4-5 under Load Case 4, respectively), illustrating that the calculated normal strain on concrete slab from FEA agreed well with the measured ones. The maximum compression stress was 4.2 MPa under eccentric loading (Load Case 4), which was much less than the designed value of concrete C50 ($f_{cd} = 22.4$ MPa) in Specification JTG D62 (Ministry of Communication of China 2012), which confirmed that the concrete slab had enough flexural strength.

The normal strain on the bottom of the steel tube at midspan (Section 3) under Load Cases 2 and 4 are also given in Fig. 15. The steel tube was in tension, and the η of normal strain changed from 0.92 to 1.09 (the minimum and maximum η were obtained from the steel strain of G3-2 under Load Case 4 and G3-5 under Load Case 4, respectively), indicating that the calculated normal strain on steel tube from FEA coincided with the measured ones. Steel strain under eccentric loading was increased by about 20% in comparison to that under symmetrical loading. The maximum normal stress on steel tube was 51 MPa under eccentric loading (Load Case 4), and it was much less than the yield stress of steel Q355 ($f_y = 55$ MPa), which confirmed that the steel tube had enough strength margin. We did not

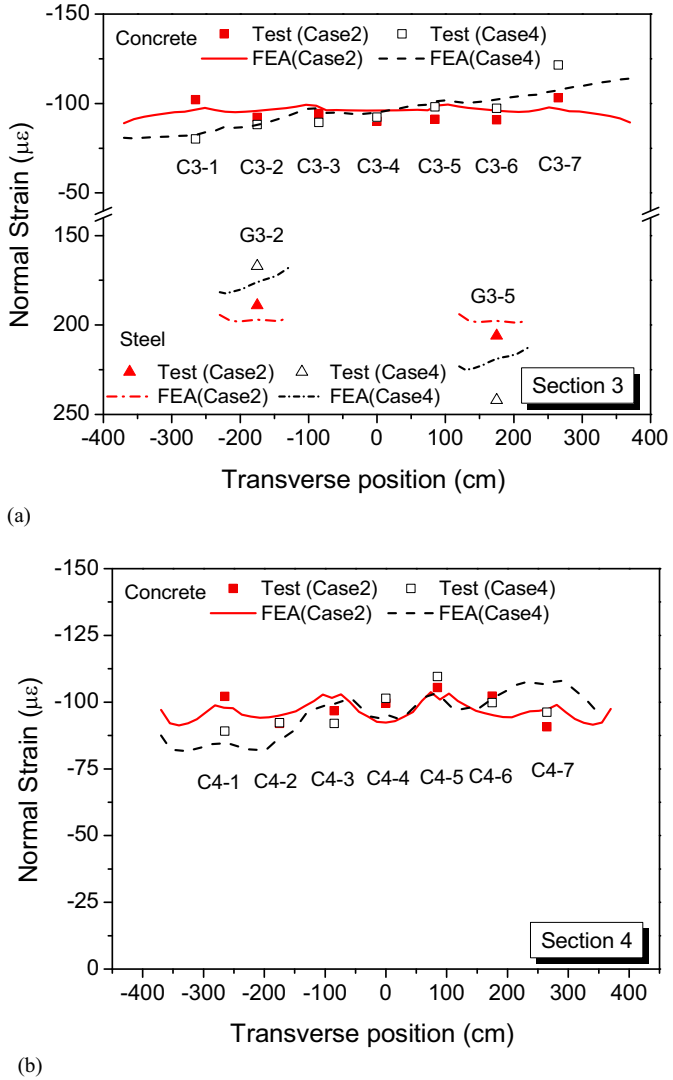

Fig. 15. Normal strain on the slabs (field test) in (a) Section 3; and (b) Section 4.

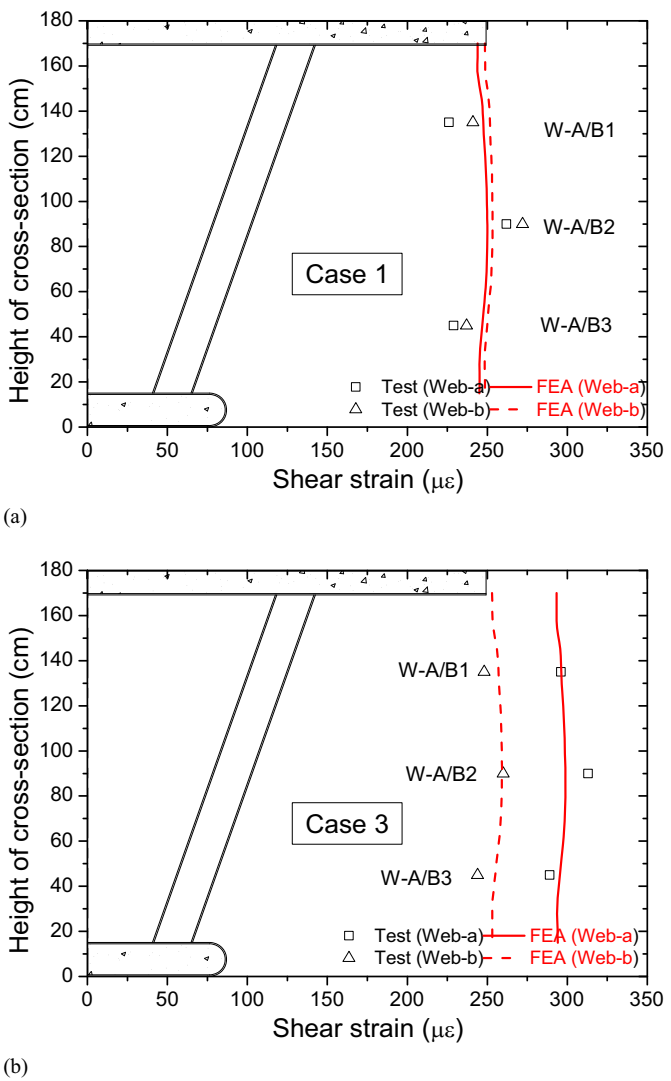

Fig. 16. Shear strain on corrugated steel webs (field test): (a) Load Case 1; and (b) Load Case 3.

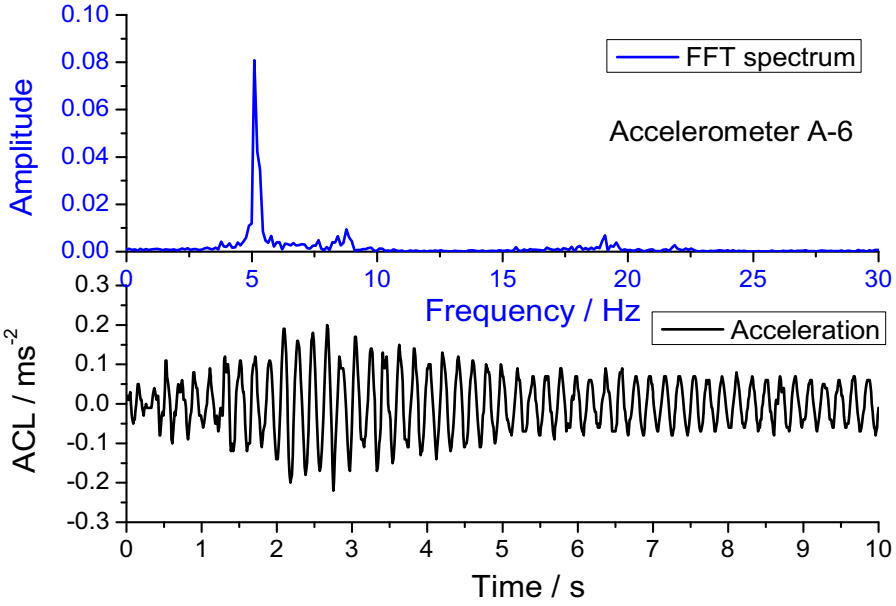

Fig. 17. FFT spectrum obtained from acceleration response for ambient vibration. ACL = acceleration.

Table 3. Dynamic characteristics

Mode	Test		FEA
	Frequency (Hz)	Damping ratio (%)	Frequency (Hz)
1st: Vertical symmetric flexure	5.10	1.28	5.04
2nd: Symmetric torsion	8.77	3.78	8.75
3rd: Vertical antisymmetric flexure	16.41	7.42	16.04
4th: Antisymmetric torsion	19.54	1.47	21.10

measure the strain of concrete inside the steel tube during field load test, but if we assume that the strain at bottom layer of concrete inside the steel tube is the same as the strain at the bottom of steel tube (242 $\mu\varepsilon$ at G3-5 under Load Case 4), which is larger than tensile cracking strain (52 $\mu\varepsilon$), the concrete will crack without application of prestressing. In order to prevent concrete cracking at the bottom slab, prestressing is necessary to arrange in the concrete-filled steel tube.

Shear Strain on Corrugated Webs

Since most of the shear loading was resisted by the web, we observed the shear strain of corrugated steel webs near the support area (Section 1) under Load Cases 1 and 3 to check the strength and stability, as given in Fig. 16. The calculated shear strain distributed almost uniformly along the height of the web, while the measured shear strain at the center was slightly larger than that at top and bottom of the webs, which may be caused by the following reasons: (1) we did not consider geometric imperfections of thin corrugated steel web due to processing and transportation in the FE model; (2) we did not consider the residual stress caused by welding connection between web and flange plate in numerical analysis; (3) we assumed the steel–concrete interface between concrete slab and top steel plate, infill concrete, and steel tube to be a fully rigid connection in the FE simulation.

The η of the shear strain changed from 0.91 to 1.08 (the minimum and maximum η were obtained from the shear strain of W-

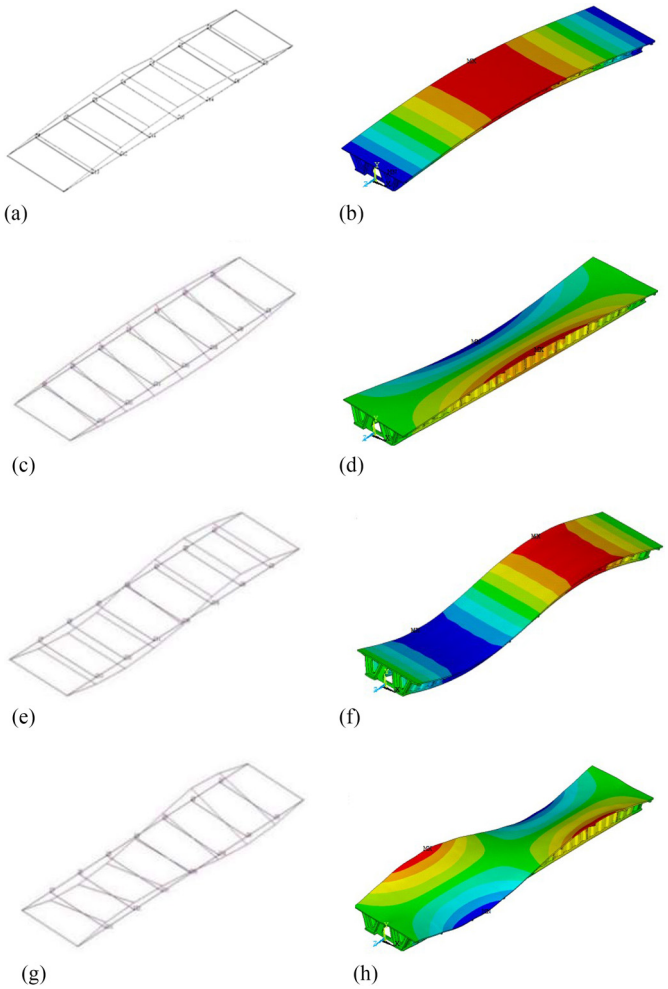

Fig. 18. Mode shape: (a) Test First Order; (b) FEA First Order; (c) Test Second Order; (d) FEA Second Order; (e) Test Third Order; (f) FEA Third Order; (g) Test Fourth Order; and (h) FEA Fourth Order.

B3 under Load Case 3 and W-B2 under Load Case 1, respectively), confirming that the calculated shear strain of corrugated steel web from FEA agreed well with the measured ones. Also, the maximum shear stress was 24 MPa under eccentric loading (Load Case 3), which was much less than the yield shear stress of steel Q355 ($\tau_y = 355/\sqrt{3} = 205$ MPa), which demonstrated that the corrugated steel web has enough shear strength. The effect of unbalanced load on the shear strain of corrugated steel web can be reflected by the ratio of maximum strain under eccentric loading to the average one under symmetrical loading (299 $\mu\varepsilon$/252 $\mu\varepsilon$ = 1.20); the increment of 20% was caused by the eccentric loading.

Previous load-carrying capacity test results confirm that the bending moment and axial force on the composite girder with corrugated steel webs are carried by the top and bottom flanges, and most of the shear force is carried by the webs; the shear stress distributes uniformly along the height of the web. We calculated the shear stress under Load Case 1 as 22 MPa under the assumption that all shear force was carried by corrugated steel web. In comparison with the average tested shear stress (about 20 MPa) under the same load case, it can be found that approximately 90% of the shear force was resisted by corrugated steel webs in the researched bridge. Therefore, the shear force of the composite girder can be easily and conservatively predicted using the shear strength of corrugated steel webs and neglecting the contribution of the slabs.

Dynamic Testing Results

Frequencies and Mode Shapes

We conducted ambient vibration testing to measure dynamic characteristics. We measured the responses of the bridge were measured through 14 accelerometers with a higher-quality property of lower frequency; the locations of each accelerometer are given in Fig. 11(d). The acceleration response of Accelerometer A-6 and its magnitude of the power spectrum by fast Fourier-transform (FFT) technique obtained from ambient vibration on the bridge are given in Fig. 17.

Measured and calculated frequencies and mode shapes are compared in Table 3 and Fig. 18. We obtained a good agreement between experimental natural frequencies, mode shapes, and numerical ones. The mean value of the ratio of experimental natural frequencies to FEA ones is 0.98 with a standard deviation of 0.04. It should be noted that higher modal frequencies could not be obtained because of difficulty associated with exciting higher modes during ambient vibration testing. The tested damping ratio of such composite bridge was between the general value of the concrete bridges and the value of the steel bridges.

Dynamic Load Factor

The DLF was determined by dividing the measured maximum dynamic response ($R_{dyn.}$) to the known static response ($R_{stat.}$) in terms of the normal strain or the deflections at selected locations of the tested bridge.

Typical dynamic and static responses for calculating the DLF were obtained from the deflection (LVDT D4-1) under a three-axle truck with a speed of 40 km/h, as given in Fig. 19. The DLF under load cases of truck jumping and braking are also presented.

Fig. 20 summarizes the DLF form the measured normal strain at both top and bottom slabs, as well the displacement at the bottom slab under moving of the truck with the speeds of 20, 30, and 40 km/h, and jumping and braking of the truck. The DLF reduced slightly as the speed increased under the case of truck moving. The maximum DLF occurred in the case of truck jumping, which can be assumed as the upper limit of the DLF, considering the impact effect.

We summarized the code-based DLFs and compared to the field test results, as listed in Table 4. The average DLF obtained from the test (except the load case of truck jumping) is less than the values obtained from the design codes: Load resistance factor design (LRFD) (AASHTO 2010), BS 5400 (BSI 1978), BD 37/01 (British Dept. for Transport 2001), JTG D62 (Ministry of Communication of China 2012), and JRA (2002). The specification BD 37/01 predicts the DLF most conservatively. Therefore, the DLF of prefabricated composite box girder bridge

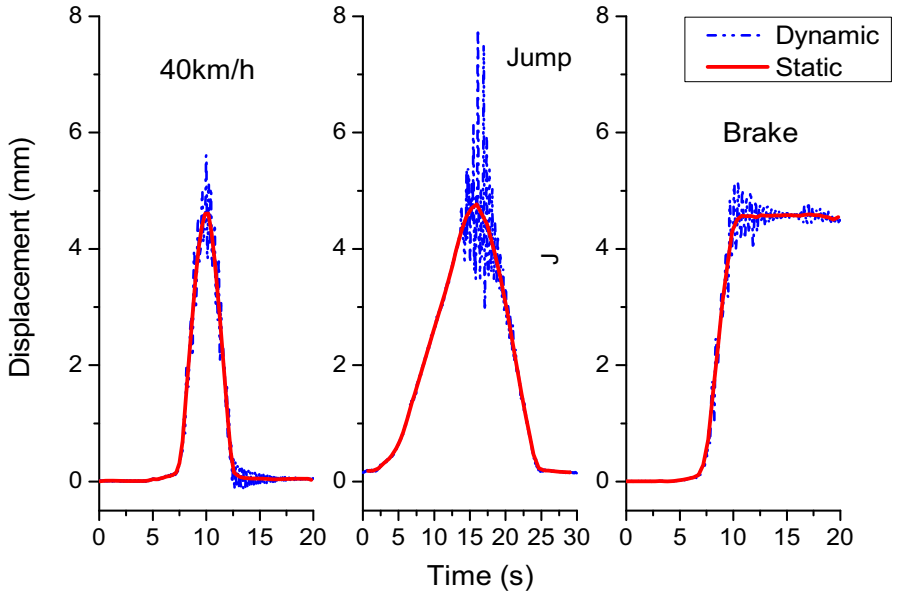

Fig. 19. Typical responses for computing dynamic load factor.

J. Bridge Eng., 2019, 24(6): 04019047

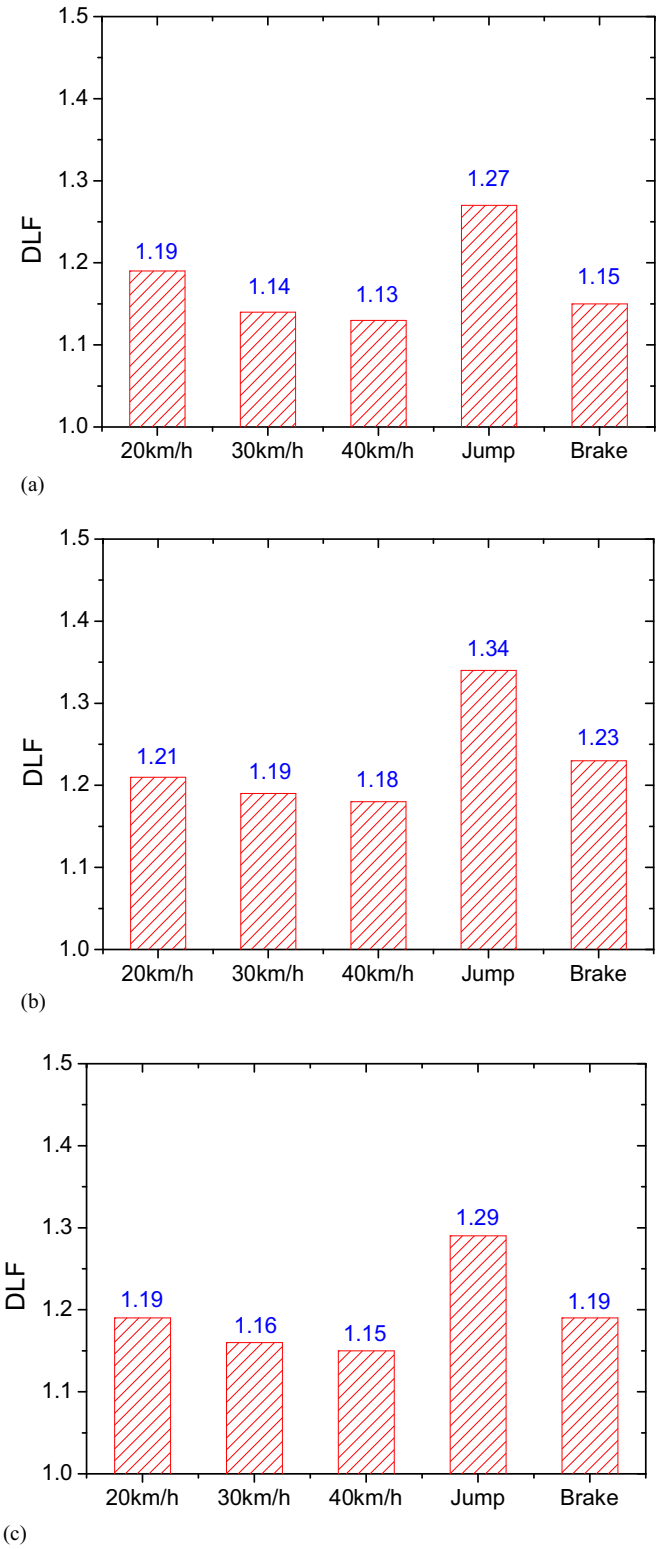

Fig. 20. Dynamic load factors from live-load field test from: (a) normal strain at top slab; (b) normal strain at bottom slab; and (c) displacement at bottom slab.

with corrugated webs can be appropriately predicted by the recommendation in the aforementioned design codes except BD 37/01.

Table 4. Summary of DLF according to different design codes and test results

Parameter	DLF
Design code	
AASHTO (LRFD)[a]	1.33
BS 5400[b]	1.25
BD 37/01[c]	1.80
JTJ D60-2004[d]	1.272
JRA 2002	1.25
Test results (average)	
Moving	1.17
Jumping	1.3
Braking	1.19

[a]AASHTO 2010.
[b]BSI 1978.
[c]British Dept. for Transport 2001.
[d]Ministry of Communication of China 2012.

Structural Performance Analysis and Evaluation

Simplified Analysis of Flexural and Shear Strength

Flexural Strength

On the basis of previous studies (Mo and Fan 2006; He et al. 2014a, b) and experimental results of the fabricated composite box girder with corrugated steel webs, some assumptions were proposed for the analytical model to predict flexural resistance:

1. Since relative slip at the steel–concrete interface between concrete and steel plate is less than 0.1 mm before steel yielding, a full connection is achieved between concrete and steel plates for the composite deck and concrete-filled steel tube; the normal strain of the slabs changes linearly along the height, satisfying the plane section (only slabs without corrugated steel webs in section) assumption.
2. The nonlinear model (a parabolic curve) is adopted for the relationship between the stress (f_c) and strain (ε_c) of concrete in compression. On the tensile side, a linear model is adopted for the relationship between the stress and strain. After crack resistance strength (f_{tr}), the contribution of cracked concrete in tension to flexure strength is ignored.
3. The elastic–perfectly plastic model is used for steel and prestressed tendon. A linear model is adopted for the relationship between the stress and strain up to the yield stress; afterward, stress keeps constant while strain still increases, and tension-stiffening effect is not considered.

A simplified analytical method has been proposed to calculate the bending strength of composite girder with corrugated steel webs using a multiple layers model. Only the top and bottom slabs are considered in the cross section to resist bending moment.

The ultimate state is defined as the yield stress of the steel tube (f_y), and the prestressed tendon (f_{py}) is attained; the compressive concrete stress reaches to maximum strength (f'_c). The ultimate bending moment M_u is calculated based on the full plastic section. The distribution of strain and stress is given in Fig. 21, in which A_p, A_{bs}, and A_{ts} are the areas of prestressed steel tendon and steel plates of bottom and top slabs; f_p, f_{bs}, and f_{ts} are the yield stress of prestressed steel tendon and steel plates of bottom and top slabs; A_{tc} and f'_s are the area and compressive strength of the concrete deck; and h, h_f, and h'_f are the height of the composite girder, steel tube, and composite deck.

$$M_u = (A_p f_{py} + A_{bs} f_y)\left(h - h_f/2 - h'_i/2\right) \quad (1)$$

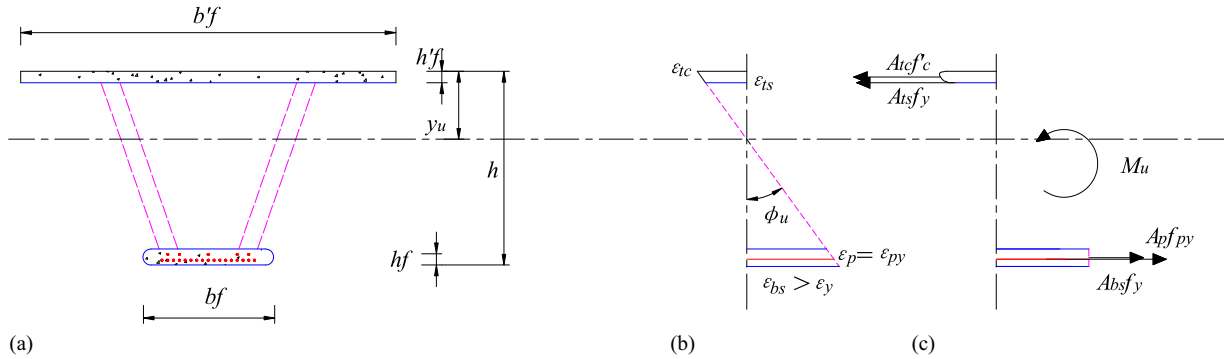

Fig. 21. Flexural strength analysis under ultimate state: (a) cross section; (b) strain; and (c) stress and force.

The analytical flexural strength using the simplified calculation method is 18,937 kN·m, slightly more (2%) than the tested ultimate moment (18,560 kN·m), which indicates the proposed simplified analytical method can be used to predict the ultimate flexural strength of such composite girder.

Shear Strength

The vertical shear force is assumed to be resisted by corrugated steel webs, neglecting the contribution of the top and bottom slabs, which is conservative in the safe side for the design of corrugated steel webs. Moreover, the shear strength of the composite girder is controlled by shear buckling or yielding of the corrugated steel web. Generally, the corrugated steel web should be designed to avoid buckling before steel yielding. Shear stress distributes almost uniformly, which can be taken as a constant over the height. Therefore, shear force (V_s) for such composite girder section can be predicted as follows:

$$V_s = \tau_y h_w t_w \tag{2}$$

where h_w and t_w = vertical height and thickness of corrugated steel webs; and τ_y = yield shear stress. The calculation method of shear strength for corrugated steel webs had been verified by many researchers (Elgaaly et al. 1996; Sause and Braxtan 2011; He et al. 2012b, c).

Bridge Performance Evaluation

Condition assessment and safety verification of existing bridges and the decisions as to whether a bridge requires posting currently are addressed through analysis, load testing, or a combination of these methods (Wang et al. 2011). The rating process is described in AASHTO's *Manual for Bridge Evaluation* (AASHTO 2003), which permits ratings to be determined by the load and resistance factor (LRF) methods. The ratings were conducted using LRF rating (LRFR) method at three levels: the design loads, the AASHTO/state legal loads, and the permitted loads. This study chose the third level, the permitted live load (48-ton truck in calibration test). The load ratings are determined by

$$R_F = \frac{R_n - \gamma_D D}{\gamma_L L(1+I)} \tag{3}$$

where R_F = bridge load rating (operating or inventory) factor; R_n = nominal flexure or shear capacity, γ_D = dead load factor (1.3); γ_L = live-load factor (1.3 for operating, 2.17 for inventory); D = nominal dead load effect, L = nominal live-load effect; and I = live-load impact factor.

Table 5. AASHTO LRFD load rating results

	Load rating	
Strength	Inventory	Operating
Flexural	1.35	2.25
Shear	2.30	3.85

The operating and inventory load ratings were calculated based on analytical flexure or shear capacity [Eqs. (1) and (2)] and field load test results (I = 0.3 and eccentric load factor = 1.2); these ratings are provided in Table 5. According to the AASHTO LRFD load rating method, this kind of bridge is capable of bearing a load of the 48-ton truck in the calibrating test because their load ratings are more than one, and the control load capacity is the flexural strength (AASHTO 2010).

Conclusions

This paper presents an experimental and analytical investigation on the static and dynamic performance of a prefabricated composite box girder bridge with corrugated webs and concrete-filled steel tube slabs before and after erection through a full-scale model test and live-load field tests. The following conclusions can be drawn from the present study:

1. The model test results show that the steel yielding load was 5.5 and 2 times the design load and serviceability load, while the deflection at steel yielding state was 13 and 3 times that at design and serviceability states, respectively, which confirms the prefabricated composite box girder has enough loading capacity and sufficient ductility.
2. In the calibration test, the maximum deflection, normal stress on slabs, and shear stress on corrugated webs were much less than the required values under the serviceability state, which confirmed that the tested bridge had enough stiffness and strength. The diaphragms were beneficial to distribute live loads, especially under the eccentric load condition, because lateral stiffness is improved by connecting two box girders together using the diaphragms.
3. In the dynamic load test, the DLF reduced slightly with the increased speed of moving truck. And the DLF can be appropriately predicted by the design codes [AASHTO 2010, BS 5400 (BSI 1978), JTJ D60-2004 (Ministry of Communication of China 2012), JRA 2002] except BD 37/01 (British Dept. for Transport 2001).
4. The experimental and numerical results indicate that the flexural strength is almost resisted by the top slab and bottom

concrete-filled steel tube without considering the contribution of corrugated steel web due to its accordion effect, but the shear force is mostly resisted by the corrugated steel web.

5. The inventory and operating load rating factors in terms of flexural and shear strength are more than one, indicating that such kind of bridge can be capable of bearing the load of the 48-ton truck in the calibrating test with a sufficient safety margin.

All the findings from static and dynamic load tests in this study may provide a reference for the design and construction of such type bridges. Since the stress state of infill concrete and prestressed strands were not measured in present study, the stress control of infill concrete and stress developed from prestressed strands during various loading stages will be further investigated experimentally and numerically.

Acknowledgments

This research is sponsored by the National Nature Science Foundation of China under Grant 51578406 and 51308070, and the Science And Technology Project of the Ministry of Transport under Grant 2013318822370. The authors express their gratitude for this support. The authors would like to thank Prof. George Vasdravellis in Heriot-Watt University, United Kingdom, and Dr. Zhan Lyu in Imperial College London, United Kingdom, for their help and suggestions revising this paper.

References

AASHTO. 2003. *Guide manual for condition evaluation and load and resistance factor rating (LRFR) of highway bridges.* 1st ed. (including 2005 Interim Revisions). Washington, DC: AASHTO.

AASHTO. 2010. *LRFD bridge design specifications.* 5th ed. Washington, DC: AASHTO.

Anami, K., and R. Sause. 2005. "Fatigue of web-flange weld of corrugated web girders: 2. Analytical evaluation of fatigue strength of corrugated web flange weld." *Int. J. Fatigue* 27 (4): 383–393. https://doi.org/10.1016/j.ijfatigue.2004.08.007.

Anami, K., R. Sause, and H. H. Abbas. 2005. "Fatigue of web-flange weld of corrugated web girders: 1. Influence of web corrugation geometry and flange geometry on web-flange weld toe stresses." *Int. J. Fatigue* 27 (4): 373–381. https://doi.org/10.1016/j.ijfatigue.2004.08.006.

Ashebo, D. B., T. H. T. Chan, and L. Yu. 2007. "Evaluation of dynamic loads on a skew box girder continuous bridge Part I: Field test and modal analysis." *Eng. Struct.* 29 (6): 1052–1063. https://doi.org/10.1016/j.engstruct.2006.07.014.

Ayyub, B. M., Y. G. Sohn, and H. Saadatmanesh. 1992. "Prestressed composite girders. I: Experimental study for negative moment." *J. Struct. Eng.* 118 (10): 2743–2762. https://doi.org/10.1061/(ASCE)0733-9445(1992)118:10(2743).

British Dept. for Transport. 2001. *Loads for highway bridges.* BD 37/01. London: British Dept. for Transport.

BSI (British Standards Institution). 1978. *BS 5400. Steel, concrete and composite bridges. Part 2. Specification for loads.* London: BSI.

Brozzetti, J. 2000. "Design development of steel-concrete composite bridges in France." *J. Constr. Steel Res.* 55 (1-3): 229–243. https://doi.org/10.1016/S0143-974X(99)00087-5.

Cai, C. S., and M. Shahawy. 2003. "Understanding capacity rating of bridges from load tests." *Pract. Period. Struct. Des. Constr.* 8 (4): 209–216. https://doi.org/10.1061/(ASCE)1084-0680(2003)8:4(209).

Chen, H. 2013. "Bearing capacity test and calculation method study on innovative steel-concrete composite box girder bridge." M.A. thesis, Dept. of Bridge Engineering, Tongji Univ.

Chen, S., and P. Gu. 2005. "Load carrying capacity of composite beams prestressed with external tendons under positive moment." *J. Constr. Steel Res.* 61 (4): 515–530. https://doi.org/10.1016/j.jcsr.2004.09.004.

Cheyrezy, M., and J. Combault, 1990. "Composite bridges with corrugated steel webs - Achievements and prospects." In *Proc., IABSE Symp., Mixed Structures and New Materials*, 479–484. Brussels: IABSE.

Ding, Y., K. Jiang, and Y. Liu. 2012. "Nonlinear analysis for PC box-girder with corrugated steel webs under pure torsion." *Thin-Walled Struct.* 51: 167–173. https://doi.org/10.1016/j.tws.2011.10.013.

Driver, R. G., H. H. Abbas, and R. Sause. 2006. "Shear behavior of corrugated web bridge girders." *J. Struct. Eng.* 132 (2): 195–203. https://doi.org/10.1061/(ASCE)0733-9445(2006)132:2(195).

El Hadidy, A., M. F. Hassanein, and M. Zhou. 2018. "The effect of using tubular flanges in bridge girders with corrugated steel webs on their shear behaviour – A numerical study." *Thin-Walled Struct.* 124: 121–135. https://doi.org/10.1016/j.tws.2017.11.050.

Elamary, A., M. M. Ahmed, and A. M. Mohmoud. 2017. "Flexural behaviour and capacity of reinforced concrete-steel composite beams with corrugated web and top steel flange." *Eng. Struct.* 135: 136–148. https://doi.org/10.1016/j.engstruct.2017.01.002.

Elgaaly, M., R. W. Hamilton, and A. Seshadri. 1996. "Shear strength of beams with corrugated webs." *J. Struct. Eng.* 122 (4): 390–398. https://doi.org/10.1061/(ASCE)0733-9445(1996)122:4(390).

Elgaaly, M., A. Seshadri, and R. W. Hamilton. 1997. "Bending strength of steel beams with corrugated webs." *J. Struct. Eng.* 123 (6): 772–782. https://doi.org/10.1061/(ASCE)0733-9445(1997)123:6(772).

Eom, J., and A. S. Nowak. 2001. "Live load distribution for steel girder bridges." *J. Bridge Eng.* 6 (6): 489–497. https://doi.org/10.1061/(ASCE)1084-0702(2001)6:6(489).

He, J., Y. Liu, A. Chen, D. Wang, and T. Yoda. 2014a. "Bending behavior of concrete-encased composite I-girder with corrugated steel web." *Thin-Walled Struct.* 74 (9): 70–84. https://doi.org/10.1016/j.tws.2013.08.003.

He, J., Y. Liu, A. Chen, and T. Yoda. 2012a. "Mechanical behavior and analysis of composite bridges with corrugated steel webs: State-of-the-art." *Int. J. Steel Struct.* 12 (3): 321–338. https://doi.org/10.1007/s13296-012-3003-9.

He, J., Y. Liu, A. Chen, and T. Yoda. 2012b. "Shear behavior of partially encased composite I-girder with corrugated steel web: Experimental study." *J. Constr. Steel Res.* 77: 193–209. https://doi.org/10.1016/j.jcsr.2012.05.005.

He, J., Y. Liu, Z. Lin, A. Chen, and T. Yoda. 2012c. "Shear behavior of partially encased composite I-girder with corrugated steel web: Numerical study." *J. Constr. Steel Res.* 79: 166–182. https://doi.org/10.1016/j.jcsr.2012.07.018.

He, J., Y. Liu, X. Xu, and L. Li. 2014b. "Loading capacity evaluation of composite box girder with corrugated webs and steel tube slab." *Struct. Eng. Mech.* 50 (4): 501–524. https://doi.org/10.12989/sem.2014.50.4.501.

He, J., S. Wang, Y. Liu, Z. Lyu, and C. Li. 2017. "Mechanical behavior of partially encased composite girder with corrugated steel web: Interaction of shear and bending." *Eng.* 3 (6): 806–816. https://doi.org/10.1016/j.eng.2017.11.005.

Huang, L., H. Hikosaka, and K. Komine. 2004. "Simulation of accordion effect in corrugated steel web with concrete flanges." *Comput. Struct.* 82 (23-26): 2061–2069. https://doi.org/10.1016/j.compstruc.2003.07.010.

Ibrahim, S. A., W. W. El-Dakhakhni, and M. Elgaaly. 2006. "Fatigue of corrugated-web plate girders: Experimental study." *J. Struct. Eng.* 132 (9): 1371–1380. https://doi.org/10.1061/(ASCE)0733-9445(2006)132:9(1371).

Jiang, R., F. T. K. Au, and Y. Xiao. 2015. "Prestressed concrete girder bridges with corrugated steel webs: Review." *J. Struct. Eng.* 141 (2): 04014108. https://doi.org/10.1061/(ASCE)ST.1943-541X.0001040.

JRA (Japan Road Association). 2002. *Specifications for highway bridges.* Tokyo: JRA.

Johnson, R. P., J. Cafolla, and C. Bernard. 1997. "Corrugated webs in plate girders for bridges." *Proc. Inst. Civ. Eng. Struct. Build.* 122 (2): 157–164. https://doi.org/10.1680/istbu.1997.29305.

Kadotani, T., K. Aoki, and S. Yamanobe. 2003. "Vibration characteristics of corrugated steel web bridge: 1. Test." [In Japanese.] *J. Prestressed Concr.* 45 (2): 90–99.

Kim, K. S., D. H. Lee, S. M. Choi, Y. H. Choi, and S. H. Jung. 2011. "Flexural behavior of prestressed composite beams with corrugated

web: Part I. Development and analysis." *Composites Part B* 42 (6): 1603–1616. https://doi.org/10.1016/j.compositesb.2011.04.020.
Kosa, K., S. Awane, H. Uchino, and K. Fujibayashi. 2006. "Ultimate behavior of prestressed concrete bridge with corrugated steel webs using embedded connection." *J. Japan Soc. Civ. Eng.* 62 (1): 202–220. [In Japanese.] https://doi.org/10.2208/jsceje.62.202.
Lichtenstein, A. G. 1993. *Bridge rating through nondestructive load testing*. Final draft, NCHRP Project 12-28(13)A. Washington, DC: Transportation Research Board, National Research Council.
Luo, R., and B. Edlund. 1996. "Shear capacity of plate girders with trapezoidally corrugated webs." *Thin-Walled Struct.* 26 (1): 19–44. https://doi.org/10.1016/0263-8231(96)00006-7.
Ministry of Communication of China. 2012. *Code for design of highway reinforced concrete and prestressed concrete bridges and culverts*. JTG D62-2012. Beijing: China Communications Press.
Mo, Y. L., and Y.-L. Fan. 2006. "Torsional design of hybrid concrete box girders." *J. Bridge Eng.* 11 (3): 329–339. https://doi.org/10.1061/(ASCE)1084-0702(2006)11:3(329).
Mo, Y. L., C. H. Jeng, and H. Krawinkler. 2003. "Experimental and analytical studies of innovative prestressed concrete box-girder bridges." *Mater. Struct.* 36 (2): 99–107. https://doi.org/10.1007/BF02479523.
Mo, Y. L., C. H. Jeng, and Y. S. Chang. 2000. "Torsional behavior of prestressed concrete box-girder bridges with corrugated steel webs." *ACI Struct. J.* 97 (6): 849–859. https://doi.org/10.14359/9630.
Nakamura, S., Y. Momiyama, T. Hosaka, and K. Homma. 2002. "New technologies of steel/concrete composite bridges." *J. Constr. Steel Res.* 58 (1): 99–130. https://doi.org/10.1016/S0143-974X(01)00030-X.
Nilson, A. H. 1987. *Design of prestressed concrete.* 2nd ed. New York: John Wiley & Sons.
Ren, W.-X., I. E. Harik, G. E. Blandford, M. Lenett, and T. M. Baseheart. 2004. "Roebling suspension bridge. II: Ambient testing and live-load response." *J. Bridge Eng.* 9 (2): 119–126. https://doi.org/10.1061/(ASCE)1084-0702(2004)9:2(119).
Sause, R., H. H. Abbas, R. G. Driver, K. Anami, and J. W. Fisher. 2006. "Fatigue life of girders with trapezoidal corrugated webs." *J. Struct. Eng.* 132 (7): 1070–1078. https://doi.org/10.1061/(ASCE)0733-9445(2006)132:7(1070).
Sause, R., and T. N. Braxtan. 2011. "Shear strength of trapezoidal corrugated steel webs." *J. Constr. Steel Res.* 67 (2): 223–236. https://doi.org/10.1016/j.jcsr.2010.08.004.
Sause, R., B.-G. Kim, and M. R. Wimer. 2008. "Experimental study of tubular flange girders." *J. Struct. Eng.* 134 (3): 384–392. https://doi.org/10.1061/(ASCE)0733-9445(2008)134:3(384).
Shao, Y., and Y. Wang. 2016. "Experimental study on shear behavior of I-girder with concrete filled tubular flange and corrugated web." *Steel Compos. Struct.* 22 (6): 1465–1486. https://doi.org/10.12989/scs.2016.22.6.1465.
Shao, Y. B., and Y. M. Wang. 2017. "Experimental study on static behavior of I-girder with concrete-filled rectangular flange and corrugated web under concentrated load at mid-span." *Eng. Struct.* 130: 124–141. https://doi.org/10.1016/j.engstruct.2016.10.002.
Teixeira de Freitas, S., H. Kolstein, and F. Bijlaard. 2012. "Structural monitoring of a strengthened orthotropic steel bridge deck using strain data." *Struct. Health Monit.* 11 (5): 558–576. https://doi.org/10.1177/1475921712449507.
Teixeira de Freitas, S., H. Kolstein, and F. Bijlaard. 2017. "Fatigue assessment of full-scale retrofitted orthotropic bridge decks." *J. Bridge Eng.* 22 (11): 04017092. https://doi.org/10.1061/(ASCE)BE.1943-5592.0001115.
Wang, N., C. O'Malley, B. R. Ellingwood, and A.-H. Zureick. 2011. "Bridge rating using system reliability assessment. I: Assessment and verification by load testing." *J. Bridge Eng.* 16 (6): 854–862. https://doi.org/10.1061/(ASCE)BE.1943-5592.0000172.
Wang, S., J. He, Y. Liu, C. Li, and H. Xin. 2018. "Shear capacity of a novel joint between corrugated steel web and concrete lower slab." *Constr. Build. Mater.* 163: 360–375. https://doi.org/10.1016/j.conbuildmat.2017.12.114.
Wang, X. 2003. "Behavior of steel members with trapezoidally corrugated webs and tubular flanges under static loading." Ph.D. dissertation, Drexel Univ.
Wang, Z., and Q. Wang. 2014. "Fatigue assessment of welds joining corrugated steel webs to flange plates." *Eng. Struct.* 73: 1–12. https://doi.org/10.1016/j.engstruct.2014.04.041.
Yi, J., H. Gil, K. Youm, and H. Lee. 2008. "Interactive shear buckling behavior of trapezoidally corrugated steel webs." *Eng. Struct.* 30 (6): 1659–1666. https://doi.org/10.1016/j.engstruct.2007.11.009.